The second European Conference on the Structural Integrity of Additively Manufactured Materials

Modelling hydrogenation during cold dwell fatigue of additively manufactured titanium alloys

A. Díaz[a]*, I.I. Cuesta[a], J.M. Alegre[a]

aUniversity of Burgos, Escuela Politécnica Superior, Avenida Cantabira s/n, Burgos, 09006, Spain

Abstract

Titanium alloys are widely employed in aerospace and automotive industries where lightweight applications are required. Additive Manufacturing (AM) processes have been proposed in order to reduce material waste and optimise mechanical properties. In addition, throughout these manufacturing processes and during service life, hydrogen uptake is expected, and the corresponding modification of mechanical properties needs to be modelled. Hydrogenation process including diffusion, trapping and hydride formation in a Ti-6Al-4V alloy during cold dwell fatigue loading, a common failure mode of titanium alloys, is simulated here. All governing equations are implemented in ABAQUS user subroutines. A boundary layer approach is used to simulate how hydrogen redistribution affects hydride kinetics near a blunting crack tip, in which cyclic loading is implemented considering different dwell times. The influence of AM techniques, especially Selective Laser Melting, is expected to promote the increase in martensite phase and microstructure defects due to rapid cooling; thus, the influence of martensite volume fraction and of trapping density on hydrogen redistribution near the crack tip is analysed. The possibility to implement hydrogen and hydride-induced dilatation is also presented, as well as a hydrogen-dependent localised plasticity model. This framework facilitates the prediction of how additive manufacturing processes affect susceptibility to hydrogen embrittlement in Ti-6Al-4V components subjected to dwell fatigue.

* Corresponding author. Tel.: +34 947258923
  E-mail address: adportugal@ubu.es

1. Introduction

Hydrogen embrittlement of different alloys, e.g. high and medium-strength steels, nickel alloys or titanium alloys, involves different micro-mechanisms that have not been completely understood yet (Djukic et al., 2019), but the interaction between hydrogen transport and different microstructural features strongly affects susceptibility to this type of failure. For titanium alloys, hydrogen assisted cracking is explained by the formation of hydrides; however, this phenomenon cannot be decoupled from hydrogen diffusion and trapping. All these processes are highly influenced by the microstructure and phase composition, so different responses to hydrogen embrittlement are expected for new production techniques such as Additive Manufacturing of industrial components.

Due to its widespread use, mechanical properties of Ti-6Al-4V alloy, including fracture and fatigue behaviour, have been extensively studied considering different AM techniques, e.g. Selective Laser Melting (SLM) or Electrom Beam Melting (EBM). However, to the best of our knowledge, few works have combined the study of SLMed Ti-6Al-4V and hydrogen embrittlement (Kacenka et al., 2021; Metalnikov et al., 2021; Neikter, 2019; Silverstein & Eliezer, 2018). One of the most influential factors of SLM for hydrogen susceptibility is the appearance of α' martensite due to rapid cooling (Metalnikov et al., 2021); however, other features typical of AM are also critical for hydrogen transport and embrittlement processes: presence of residual stresses, anisotropy or porosity.

Predicting whether hydrogen transport triggers or limits hydride formation requires a transient approach within Finite Element simulations, especially to analyse the effect of strain rates or cyclic loading. Since Ti-6Al-4V consist of a α / β microstructure, diffusivity and hydrogen solubility are modelled here as a function of the phase composition. The aim of the present work is to present a robust framework to reproduce hydrogen accumulation and hydride formation near a crack tip. Section 2 presents governing equations and numerical implementation in ABAQUS subroutines. Section 3 discusses the parameter choice that can represent microstructure features of a SLMed Ti-6Al-4V and details the simulated crack geometry and loading. Finally, the effects of diffusivity, martensite fraction, trapping density and loading conditions are analysed.

2. Numerical modelling

In this work a modelling framework is presented in which the following phenomena are implemented in ABAQUS subroutines: (i) hydrogen interstitial diffusion and stress-drifted diffusion; (iii) hydrogen trapping in dislocations and grain boundaries; (ii) hydride formation kinetics; and (iv) cyclic loading (dwell fatigue) of a blunting crack tip.

2.1. Hydrogen diffusion and trapping

The governing equation for hydrogen transport is obtained from a mass balance in which hydrogen concentration in ideal lattice sites, C_L, is the dependent variable. Trapping is modelled as an extra term, $\partial C_T / \partial t$, reproducing hydrogen retention in microstructural features such as dislocations, grain boundaries and pores. This term acts as a "sink" for interstitial hydrogen and it is rewritten in (1) following (Dadfarnia et al., 2011). Here only hydrogen flux through lattice sites is modelled, resulting in a two-term flux including concentration and hydrostatic stress gradients $\nabla \sigma_h$. The latter term models the tendency of hydrogen to accumulate in tensile regions:

$$(1-f)\frac{\partial C_L}{\partial t} + \frac{K_T N_T / N_L}{\left[1+(K_T-1)C_L / N_L\right]^2}\frac{\partial C_L}{\partial t} = \nabla\left(D_L \nabla C_L - \frac{D_L C_L V_H}{RT}\nabla \sigma_h\right) \tag{1}$$

where $K_T = \exp\left(E_B / RT\right)$ is the equilibrium constant that depends on the binding energy of microstructural defects. N_T and N_L are the number of trapping and lattice sites per unit volume, respectively. Trapped hydrogen is assumed to be in thermodynamic equilibrium with lattice hydrogen. The influence of hydride formation in the balance of interstitial hydrogen is modelled following Lufrano et al., (1996) through the coefficient $(1-f)$, where f is the hydride volume fraction. V_H is the partial molar volume of hydrogen within the metal, T the temperature and R the constant of gases. Diffusivity through lattice sites depends on the fraction of each Ti phase, especially due to the much

faster diffusivity through bcc β phase than in hcp α or α'. For the sake of simplicity, here two bound limits are considered as a function of the fraction f^i and diffusivity D^i of each phase i :

$$D_L^{\square} = f^\alpha D^\alpha + f^\beta D^\beta + f^{\alpha'} D^{\alpha'} \tag{2}$$

$$D_L^{\perp} = \left(f^\alpha / D^\alpha + f^\beta / D^\beta + f^{\alpha'} / D^{\alpha'} \right)^{-1} \tag{3}$$

Anisotropy due to building direction in SLM will result in different microstructure arrays, tending to a "shortcut" parallel transport, i.e. $D_L^{\square}$, or to a slower diffusion perpendicular to the layered microstructure, i.e. $D_L^{\perp}$. The concentration imposed in the crack boundary B is proportional to an equilibrium concentration C_L^0, that depends on the charging conditions from environment, but it also should include the hydrostatic stress on the crack surface:

$$C_L(\mathrm{B}) = C_L^0 \exp\left(\frac{V_H \sigma_h}{RT}\right) \tag{4}$$

Diffusion and trapping expressions are implemented in a UMATHT subroutine, exploiting the analogy between hydrogen transport and heat transfer. The corresponding boundary condition expressed in (4) is applied to the 11 degree of freedom in ABAQUS, i.e. the temperature d.o.f., through a DISP subroutine. To access the nodal values of σ_h a URDFIL subroutine is used. More details can be found in (Díaz et al., 2016).

2.2. Hydride formation

The present kinetic and thermodynamic framework follows the model proposed by Lufrano et al. (1996). Hydride formation is modelled through the evolution of f and considering solute hydrogen concentration c_s in hydrogen atoms per solid solution atoms, i.e. $c_s = C_L / (C_L + N_A / V_M)$, where N_A is the Avogadro's number and V_M the molar volume of titanium:

$$\frac{\partial f}{\partial t} = \begin{cases} 0 & c_s < c_s^\sigma \\ \left(1 + \frac{(1 - c_s^\sigma)(1 - 2c_s)V_M}{(c_s - c_s^\sigma)V_{hr}} \right)^{-1} & c_s^\sigma \le c_s < c_h \\ 1 & c_h \le c_s \end{cases} \tag{5}$$

where V_{hr} is the partial molar volume of forming hydrides and c_h the concentration above which all solute hydrogen becomes part of the hydride phase, here equal to 2/3 for the MH_2 δ -Ti hydride. The terminal solid solubility c_s^σ influences hydride formation and depends on hydrostatic stress and on hydrogen/metal concentration $a = c_s / (1 - c_s)$. A rule of mixtures is also assumed to determine the solubility c_s^0 in the absence of stresses, where c_s^i is the hydrogen solubility in each phase i :

$$c_s^\sigma = \left(f^\alpha c_s^\alpha + f^\beta c_s^\beta + f^{\alpha'} c_s^{\alpha'} \right) \exp\left[\frac{\sigma_h}{RT(1-a)} \left(V_{hr} - (V_M + aV_H) \right) \right] \tag{6}$$

Hydride formation is implemented taking advantage of state variables (STATEVS) in the UMATHT subroutine. To solve the variable f using equation (5) a forward Euler scheme is chosen as in Lufrano et al. (1996).

3. Crack tip modelling

3.1. Geometry and loading

With the aim of exploring transient effects on hydrogen assisted fracture, a typical boundary layer approach is simulated: a blunting crack tip is modelled with an initial crack tip opening $b_0 = 10$ μm, and a remote boundary radius $r = 0.15$ m. Far-field displacements from Linear Elastic Fracture Mechanics are applied using a DISP subroutine for the 2D simulated geometry (Díaz et al., 2016). Quadratic elements with reduced integration and for plane strain are chosen (CPE8RT) and a biased mesh is considered with element length of 1 μm at the crack tip. Cyclic load is modelled between $K_{min} = 4$ and $K_{max} = 40$ MPa·m$^{0.5}$, with a dwell time of 60 s, loading/unloading times of 2 s, and a rest time of 10 s at K_{min} (see Fig. 1d). Automatic increments are optimised for the transient coupled analysis using the utility PNEWDT within the UMATHT subroutine, so loading-unloading effects are captured. Young modulus $E = 117$ GPa and Poisson's coefficient $\nu = 0.34$ are chosen. A classical J2 plasticity is considered and isotropic hardening is assumed to follow a power-law hardening with an initial yield strength of 980 MPa and a hardening exponent of 0.1. Dilatation and hydrogen-enhanced local softening are not here simulated. However, strain dilatation modelling following (Lufrano et al., 1996, 1998) can be easily implemented through a UEXPAN subroutine, as proposed in (Díaz et al., 2016); similarly, a softening law dependent of hydrogen solute concentration, inspired by the hydrogen-enhanced localised plasticity (HELP) theory, can be coded in a UHARD subroutine.

3.2. Parameters and influence of Additive Manufacturing

Hydrogen diffusivity of each Ti phase is extracted from the work of (Luo et al., 2006): $D^\alpha = 1.7 \times 10^{-15}$ m^2/s and $D^\beta = 2.8 \times 10^{-12}$ m^2/s at 300 K. Diffusivity through martensite is assumed as $D^{\alpha'} = D^\alpha$. Solubilities in each phase are chosen from (Metalnikov et al., 2021): $c_s^\alpha = 0.067$, $c_s^\beta = 0.5$ and $c_s^{\alpha'} = 0.05$. The phase composition verifies the condition $f^\alpha + f^\beta + f^{\alpha'} = 1$ and it is assumed that $f^\alpha = f^\beta$. According to Waisman et al. (1973), V_H is expected to vary slightly with the stress state, hydrogen concentration or temperature, so a value of 2.0×10^{-6} m^3/mol can be assumed for Ti-6Al-4V. Molar volume V_M for this alloy equals 1.06×10^{-5} m^3/mol (Lee et al., 1991), while the effective molar volume expansion from α to δ-hydride is assumed as $V_{hr} = 1.216 V_M$ according to Shen et al. (2009). The trap density as a function of dislocation density, and thus of plastic strain, $N_T^d(\rho)$, is extracted from (Yang et al., 2020); $N_L = 3.49 \times 10^{29}$ sites/m^3 is also chosen from that reference, but it must be highlighted that it would depend on crystal structure.

With the aim of analysing possible effects of SLM on microstructure and thus on hydrogen diffusion and hydride formation, four hypothetical materials are simulated with different martensite volume fractions, $f^{\alpha'} = 0.1$ or 0.5; trapping densities, $N_T = N_T^d$ or $100\, N_T^d$; and phase arrangement that result in upper or lower diffusivity bounds, $D_L^\square$ or $D_L^\perp$. Binding energy of SLM-induced defects is chosen from a detrapping energy $E_d = 52$ kJ/mol for grain boundaries and dislocations as measured by TDS in (Silverstein & Eliezer, 2018) and assuming that $E_d - E_B = 10$ kJ/mol. Room temperature is considered, $T = 300$ K, and the equilibrium concentration at the boundary C_L^0 is fixed as 1.16×10^{27} sites/m^3, while the bulk material is also assumed to be initially pre-charged, i.e. $C_L(t = 0) = C_L^0$.

4. Results and discussion

Hydrogen concentration C_L includes diffusible hydrogen in lattice sites and also H atoms forming hydrides. In Fig. 1 this concentration, normalised by the initial equilibrium concentration C_L^0, is plotted. The lower diffusivity bound $D_L^\perp$, i.e. a microstructure arrangement requiring hydrogen to diffuse through all phases, results in a very slow hydrogen accumulation in comparison to parallel diffusion, as shown in Fig. 1(a). For $D_L^\square$ values, two C_L peaks appear: the first peak is formed due to the higher amount of hydrogen that enters from the crack tip and the stress-drifted concentration; however, the second peak is promoted by the decrease in terminal solid solubility c_s^σ with tensile hydrostatic stress and the consequent hydride formation at lower concentrations. Therefore, the stress state triggers a competition between hydrogen accumulation at lattice sites in tension regions and hydride enhanced formation, producing also two plateaus of f for a low fraction of martensite $f^{\alpha'} = 0.1$. A higher fraction $f^{\alpha'} = 0.5$, termed as material SLM3 here, is expected to slow down diffusion due to the reduction in β fraction, which is

confirmed by comparing the evolution of maximum concentration in Fig. 1d; however, due to the parallel transport here considered, the effect is weak and hydride formation kinetics dominate: the region in which hydride is completely formed increases for a higher martensite content because $c_s^{\alpha'} \square \ c_s^{\beta}$, as shown in Fig. 1a, and so hydride formation is accelerated. Thus, the SLM-enhanced martensite volume fraction can be critical for hydride embrittlement of Ti-6Al-4V despite its lower diffusivity.
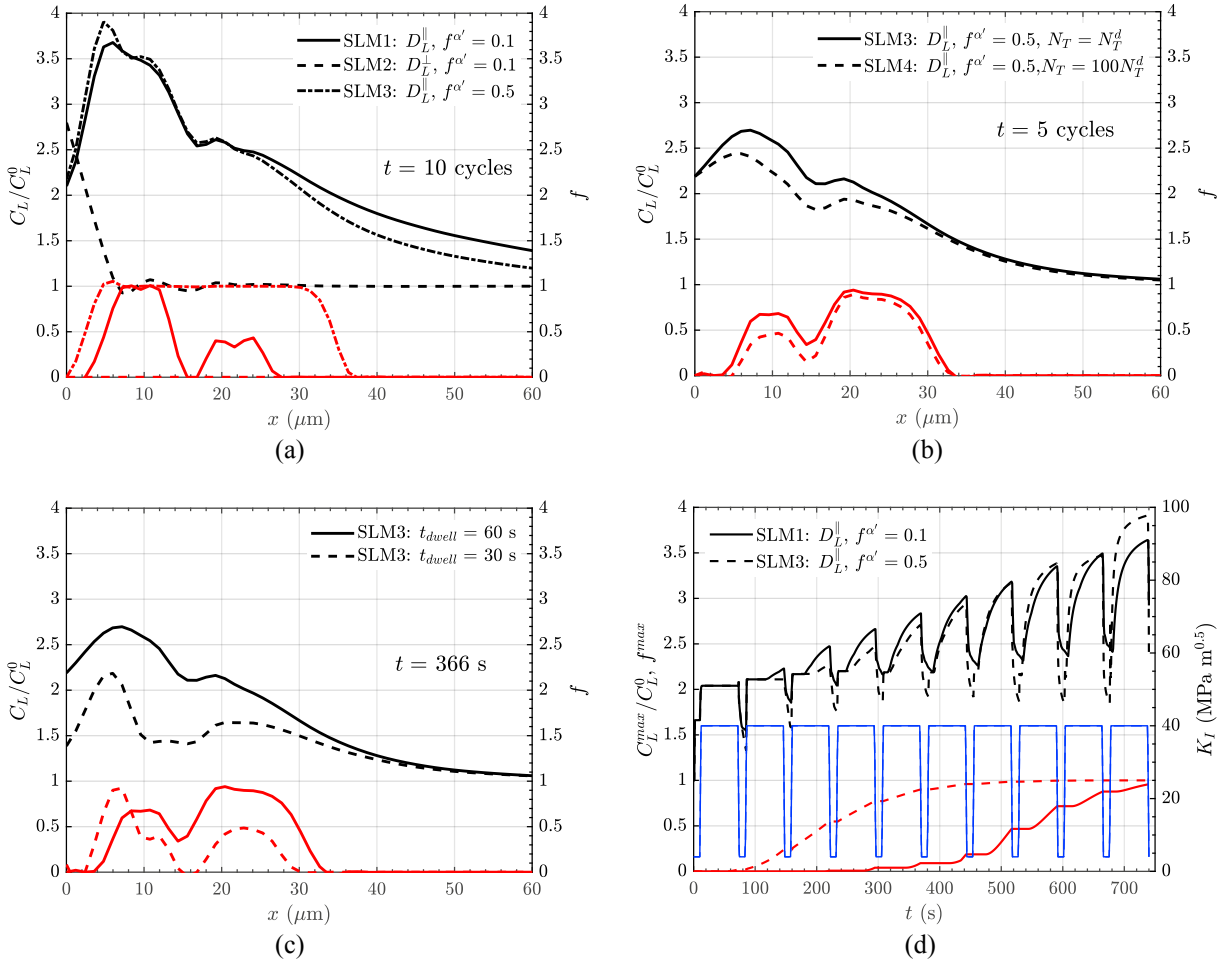
Fig. 1. Hydrogen and hydride distribution along the crack symmetry plane (a)-(c): (a) influence of diffusivity and martensite volume fraction after 10 cycles; (b) influence of trapping density after 5 cycles; (c) influence of dwell time. (d) Maximum concentration and hydride volume fraction during loading for a dwell time of 60 s.

On the other hand, Fig. 1b shows the influence of a hypothetical trapping multiplication by a factor of 100, e.g. due to an excessive distortion during cooling or to porosity defects; hydrogen retention in a higher number of traps results in a lower available lattice hydrogen and thus a lower hydride volume fraction. However, it must be noted that this phenomenon will be strongly dependents on the binding energy of traps. Finally, Fig. 1c shows the effect of a lower dwell time on hydrogen distribution: for a maximum load applied during 30 s, the attraction towards tensile regions acts during a shorter time, in comparison to a $t_{dwell} = 60$ s, and thus hydrogen accumulation and hydride formation are reduced. Here, kinematic hardening or cyclic plasticity affects are neglected, which would surely influence the interaction between hydrogen kinetics and dwell fatigue.

5. Conclusions

A numerical framework for the prediction of hydrogen accumulation and hydride formation near a crack tip has been presented. The implementation of stress-drifted and trapping-modified governing equations in ABAQUS subroutines has been demonstrated. A competition between hydrogen interstitial diffusion near the hydrostatic stress peak and the reduction in terminal solid solubility is established near a crack tip, giving rise to the corresponding hydride regions. Additionally, the possible effects of SLM in the acceleration of hydride formation have been analysed by simulating different anisotropic diffusivity bounds, martensite fractions and trap densities. Results show that SLM can enhance hydride embrittlement especially through the increase in martensite content. More complex anisotropy effects or the presence of residual stresses can easily be implemented in future research. Additionally, the present framework can be extended to include strain dilatation or hydrogen enhanced localised plasticity and can be combined with damage models to predict hydrogen embrittlement of additively manufactured Ti-6Al-4V alloys.

Acknowledgements

References

Dadfarnia, M., Sofronis, P., & Neeraj, T. (2011). Hydrogen interaction with multiple traps: Can it be used to mitigate embrittlement? *International Journal of Hydrogen Energy*, *36*(16), 10141–10148. https://doi.org/https://doi.org/10.1016/j.ijhydene.2011.05.027

Díaz, A., Alegre, J. M., & Cuesta, I. I. (2016). Coupled hydrogen diffusion simulation using a heat transfer analogy. *International Journal of Mechanical Sciences*, *115–116*. https://doi.org/10.1016/j.ijmecsci.2016.07.020

Djukic, M. B., Bakic, G. M., Sijacki Zeravcic, V., Sedmak, A., & Rajicic, B. (2019). The synergistic action and interplay of hydrogen embrittlement mechanisms in steels and iron: Localized plasticity and decohesion. *Engineering Fracture Mechanics*, *216*, 106528. https://doi.org/10.1016/J.ENGFRACMECH.2019.106528

Kacenka, Z., Roudnicka, M., Ekrt, O., & Vojtech, D. (2021). High susceptibility of 3D-printed Ti-6Al-4V alloy to hydrogen trapping and embrittlement. *Materials Letters*, *301*, 130334. https://doi.org/10.1016/J.MATLET.2021.130334

Lee, Y. T., Peters, M., & Welsch, G. (1991). Elastic moduli and tensile and physical properties of heat-treated and quenched powder metallurgical Ti-6Al-4V alloy. *Metallurgical Transactions A 1991 22:3*, *22*(3), 709–714. https://doi.org/10.1007/BF02670293

Lufrano, J., Sofronis, P., & Birnbaum, H. K. (1996). Modeling of hydrogen transport and elastically accommodated hydride formation near a crack tip. *Journal of the Mechanics and Physics of Solids*, *44*(2), 179–205. https://doi.org/http://dx.doi.org/10.1016/0022-5096(95)00075-5

Lufrano, J., Sofronis, P., & Birnbaum, H. K. (1998). Elastoplastically accommodated hydride formation and embrittlement. *Journal of the Mechanics and Physics of Solids*, *46*(9), 1497–1520. https://doi.org/http://dx.doi.org/10.1016/S0022-5096(98)00054-4

Luo, L., Su, Y., Guo, J., & Fu, H. (2006). Formation of titanium hydride in Ti–6Al–4V alloy. *Journal of Alloys and Compounds*, *425*(1–2), 140–144. https://doi.org/10.1016/J.JALLCOM.2006.01.014

Metalnikov, P., Eliezer, D., & Ben-Hamu, G. (2021). Hydrogen trapping in additive manufactured Ti–6Al–4V alloy. *Materials Science and Engineering: A*, *811*, 141050. https://doi.org/10.1016/J.MSEA.2021.141050

Neikter, M. (2019). *Microstructure and hydrogen embrittlement of additively manufactured Ti-6Al-4V*. Luleå University of Technology.

Shen, C. C., Yu, C. Y., & Perng, T. P. (2009). Variation of structure and mechanical properties of Ti–6Al–4V with isothermal hydrogenation treatment. *Acta Materialia*, *57*(3), 868–874. https://doi.org/10.1016/J.ACTAMAT.2008.10.026

Silverstein, R., & Eliezer, D. (2018). Hydrogen trapping in 3D-printed (additive manufactured) Ti-6Al-4V. *Materials Characterization*, *144*, 297–304. https://doi.org/10.1016/j.matchar.2018.07.029

Waisman, J. L., Sines, G., & Robinson, L. B. (1973). Diffusion of hydrogen in titanium alloys due to composition, temperature, and stress gradients. *Metallurgical Transactions 1973 4:1*, *4*(1), 291–302. https://doi.org/10.1007/BF02649629

Yang, F. Q., Zhan, W. J., Yan, T., Zhang, H. B., & Fang, X. R. (2020). Numerical Analysis of the Coupling between Hydrogen Diffusion and Mechanical Behavior near the Crack Tip of Titanium. *Mathematical Problems in Engineering*, *2020*. https://doi.org/10.1155/2020/3618589